CO 2 Sorption Kinetics of Scaled-Up Polyethylenimine-Functionalized Mesoporous Silica Sorbent

ARTICLE *in* LANGMUIR · MARCH 2015

Impact Factor: 4.46 · DOI: 10.1021/acs.langmuir.5b00189 · Source: PubMed

Langmuir

Article

pubs.acs.org/Langmuir

CO_2 Sorption Kinetics of Scaled-Up Polyethylenimine-Functionalized Mesoporous Silica Sorbent

M. J. Al-Marri,[†] M. M. Khader,*[,†] M. Tawfik,[†] G. Qi,[‡] and E. P. Giannelis[‡]

[†]Gas Processing Center, College of Engineering, Qatar University, P.O. Box 2713, Doha, Qatar

[‡]Department of Materials Science and Engineering, Cornell University, Ithaca, New York 14853, United States

ABSTRACT: Two CO_2 solid sorbents based on polyethylenimine, PEI (M_n ~ 423 and 10K), impregnated into mesoporous silica (MPS) foam prepared in kilogram quantities via a scale-up process were synthesized and systematically characterized by a range of analytical and surface techniques. The mesoporous silica sorbent impregnated with lower molecular weight PEI, PEI-423/MPS, showed higher capacity toward CO_2 sorption than the sorbent functionalized with the higher molecular weight PEI (PEI-10K/MPS). On the other hand, PEI-10K/MPS exhibited higher thermal stability than PEI-423/MPS. The kinetics of CO_2 adsorption on both PEI/MPS fitted well with a double-exponential model. According to this model CO_2 adsorption can be divided into two steps: the first is fast and is attributed to CO_2 adsorption on the sorbent surface; the second is slower and can be related to the diffusion of CO_2 within and between the mesoporous particles. In contrast, the desorption process obeyed first-order kinetics with activation energies of 64.3 and 140.7 kJ mol^{-1} for PEI-423/MPS and PEI-10K/MPS, respectively. These studies suggest that the selection of amine is critical as it affects not only sorbent capacity and stability but also the energy penalty associated with sorbent regeneration.

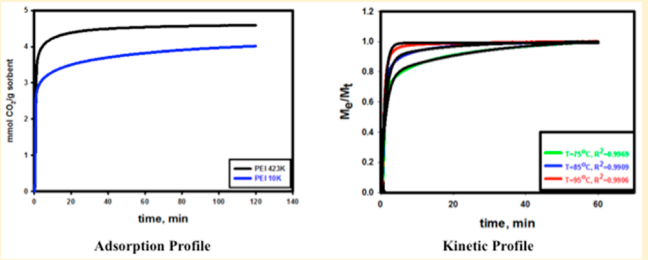

1. INTRODUCTION

Research interest in CO_2 capture has been increasingly growing over the past several years. One focus area in particular is capturing a large amount of CO_2 from dilute sources such as natural gas and power plant emissions. Several technologies have been applied to capture CO_2. Among these, amine scrubbing based on CO_2 absorption using alkanolamine solutions[1,2] is the current state-of-the-art industry process. However, the liquid phase amine scrubbing technology suffers from high regeneration cost and equipment corrosion.[3−5] As a result, there has been a strong interest to develop alternativeless energy-intensive CO_2 removal technologiess. Adsorption using solid sorbents,[6−9] particularly amine-functionalized sorbents, is appealing[10−20] due to their potentially lower energy requirements for sorbent regeneration.[5,6] By immobilizing amine functionalities on high-surface porous solid supports, the amino solid sorbents offer higher amine efficiency and thus superior sorbent performance.[17,18,21,22] Among various solid sorbent supports including zeolites,[23,24] activated carbons,[25−28] activated alumina,[29−31] and membranes,[32] mesoporous silicas have been attracting great attention.[17−19] This category of porous materials possesses several desirable properties such as large surface area, tunable pore structure, and high thermal stability. These properties make mesoporous silica a promising support for amine immobilization. To date, a series of mesoporous silicas such as MCM-417, MCM-22, MC-36, ITQ-2,[8] and many others[9] have been prepared and investigated[17−20] as supports for immobilizing various types of amines for CO_2 capture.

It is worthy to note that most of the supported amine sorbents have been synthesized on a small scale. However, economical large-scale production of supported amine sorbents is crucial for their practical CO_2 capture applications. In an effort to address this challenge, we have developed a series of cost-effective mesoporous silica foams and a scalable production process for these sorbent support.[17,33] In the present work, two solid sorbents functionalized with different polyethylenimine were prepared in kilograms using this patented scale-up process[33] and characterized by a range of analytical and surface techniques. The sorption characteristics of the CO_2 sorbents including sorbent capacity and sorption kinetics were systematically investigated. The sorption kinetics of the two sorbents were analyzed using a double-exponential model, and their sorption heats were compared to provide further insights into the sorption mechanism.

2. EXPERIMENTAL SECTION

2.1. Materials and Chemicals. Triblock copolymer poly(ethylene oxide)-*b*-(propylene oxide)-*b*-poly(ethylene oxide) surfactant P123 (EO20PO70EO20, M_n = 5800), sodium silicate, acetic acid, mesitylene, ammonium fluoride, different molecular weight polyethylenimines, PEI-423 (M_n ~ 423 g/mol, linear structure) and PEI-10K (M_n ~ 10 000 g/mol, branched structure with a ratio of primary, secondary, and tertiary amine about 1:2:1, as described by the vendor), and ethanol (v/v = 90%) were all purchased from Aldrich and used

Received: November 7, 2014
Revised: March 11, 2015
Published: March 12, 2015

DOI: 10.1021/acs.langmuir.5b00189
Langmuir 2015, 31, 3569−3576

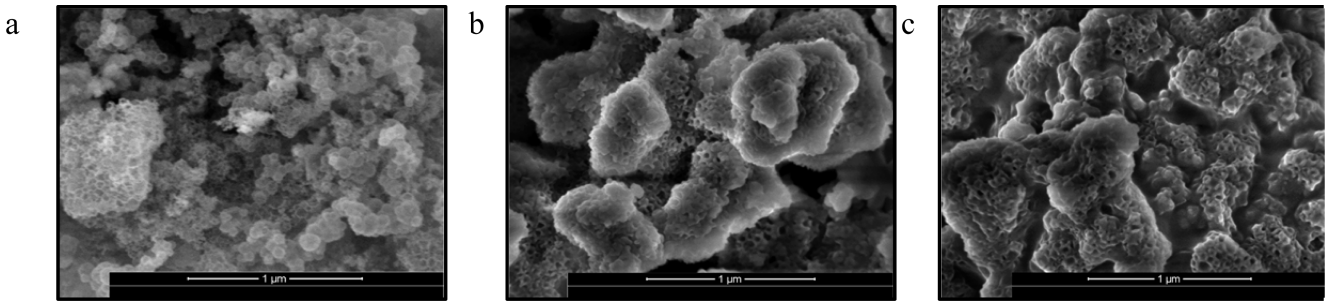

Figure 1. Scanning electron nanographs of (a) MPS, (b) PEI-423/MPS, and (c) PEI-10K/MPS.

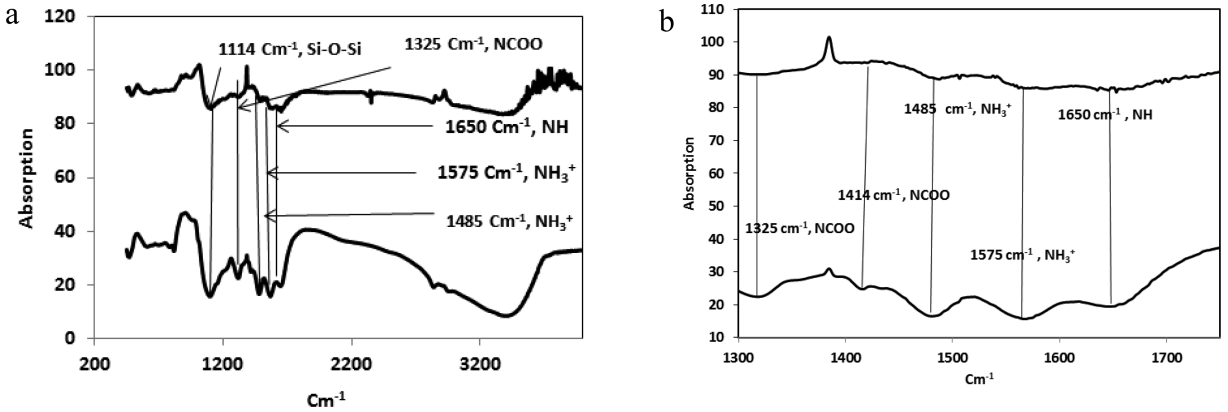

Figure 2. (a) FTIR spectra of PEI-10K/MPS before (upper curve) and after (down curve) CO_2 adsorption. (b) Detailed FTIR spectra of PEI-10K/MPS, taken from (a), before (upper curve) and after (down curve) CO_2 adsorption.

without further purification. Deionized water was used in all experiments.

2.2. Sorbent Preparation. The mesoporous silica (MPS) support was prepared in kilograms following a previously described process.[33] PEI-423 and PEI-10K were impregnated into the mesoporous silica. In a typical synthesis, a certain amount of mesoporous silica was added to 10−20 wt % PEI ethanol solution under stirring followed by statically keeping the mixture under vacuum at room temperature for 12 h. The resultant slurry was then fully dried at 80 °C for 16 h. The obtained sorbents were denoted as PEI-423/MPS and PEI-10K/MPS.

2.3. CO_2 Adsorption and Regeneration of Sorbents. As one of our focus in the study was to compare CO_2 sorption results of the scale-up synthesized sorbent to those previously obtained in a relatively small lab scale and validate the potential of scalability of our approach, a conventional gravimetric analysis technique appropriate for sorbents prepared in small amounts was used to study the sorption behavior of the sorbent. In a typical experiment ∼10 mg of sorbent was placed inside a Pyris 6 TGA PerkinElmer thermal gravimetric analyzer (TGA) furnace. To desorb any preadsorbed CO_2 and moisture, the sample was heated to 110 °C in N_2. The temperature was then kept constant until the sample mass stabilized (about 30 min). Subsequently, the sample was cooled down to the desired adsorption temperature at a cooling rate of 5 °C/min, and then a CO_2/N_2 mixture was fed to the TGA for about 2 h. The sorbent CO_2 uptake, in mmol g^{-1} sorbent, was calculated from the weight change of the sample during adsorption. The sorbent was then regenerated by flowing N_2 (99.9%) at different temperatures.

2.4. Characterization Techniques. Fourier transform infrared (FT-IR) spectra were collected on a Nicolet IS10FT-IR spectrometer with 4 cm^{-1} resolution at room temperature. A nano scanning electron microscope (NSEM) NOVANANOSEM450 was employed to investigate surface morphology and particle size. NSEM samples were prepared by dispersing a small amount of the samples in water, then dripping the dispersed samples on the NSEM holder, and leaving them to dry out under vacuum at room temperature before coating with gold. Thermal analysis was conducted using a Jade PerkinElmer differential scanning calorimeter (DSC). Samples were weighted in to standard alumina pans. A sealed empty pan was used as reference while nitrogen gas was purged at 20 mL/min during experiments. A Pyris 6 thermogravimetric analyzer (TGA) from PerkinElmer was employed for the thermal analyses from room temperature to 800 °C at a heating rate of 20 °C/min under N_2 flow.

The specific surface areas of the foam support and the sorbents were calculated by the Brunauer−Emmett−Teller (BET) method and the simplified Broekhoff−de Boer method. The total pore volume was estimated from the amount of N_2 adsorbed at a relative pressure of 0.99. The pore size and the size distribution of the foam support and the sorbents were measured by the NSEM.

Surface analysis was carried out by X-ray photoelectron spectroscopy (XPS). All XPS spectra were taken with an AXIS Ultra DLD, KRATOS apparatus equipped with an angular resolved XPS and a small spot XPS facilities. Pressure in the ultrahigh vacuum (UHV) analytical chamber during spectral acquisition was less than 5×10^{-9} Torr. The energy for survey and high-resolution scans was 80 and 20 eV, respectively. XPS analysis was carried out on the bare mesoporous silica support and PEI-423/MPS as well as PEI-10K/MPS before and after CO_2 adsorption. The samples were exposed to CO_2 in a catalytic cell under conditions similar to those of the previous TGA experiments. The catalytic cell was directly attached to the XPS UHV chamber. After treatment in CO_2, the catalytic cell was evacuated, and the samples were transferred directly to the UHV chamber without being exposed to the ambient conditions.

3. RESULTS AND DISCUSSION

3.1. Characterization of Sorbents. The BET surface area and the total pore volume of the MPS foam are 482 m^2 g^{-1} and 2.51 cm^3 g^{-1}, respectively. The cumulative surface area and the cumulative pore volume of the MPS foam calculated using the simplified Broekhoff−de Boer method are 750 m^2 g^{-1} and 2.5 cm^3 g^{-1}, respectively. The morphology of the support before and after amine impregnation was investigated by NSEM.

DOI: 10.1021/acs.langmuir.5b00189
Langmuir 2015, 31, 3569−3576

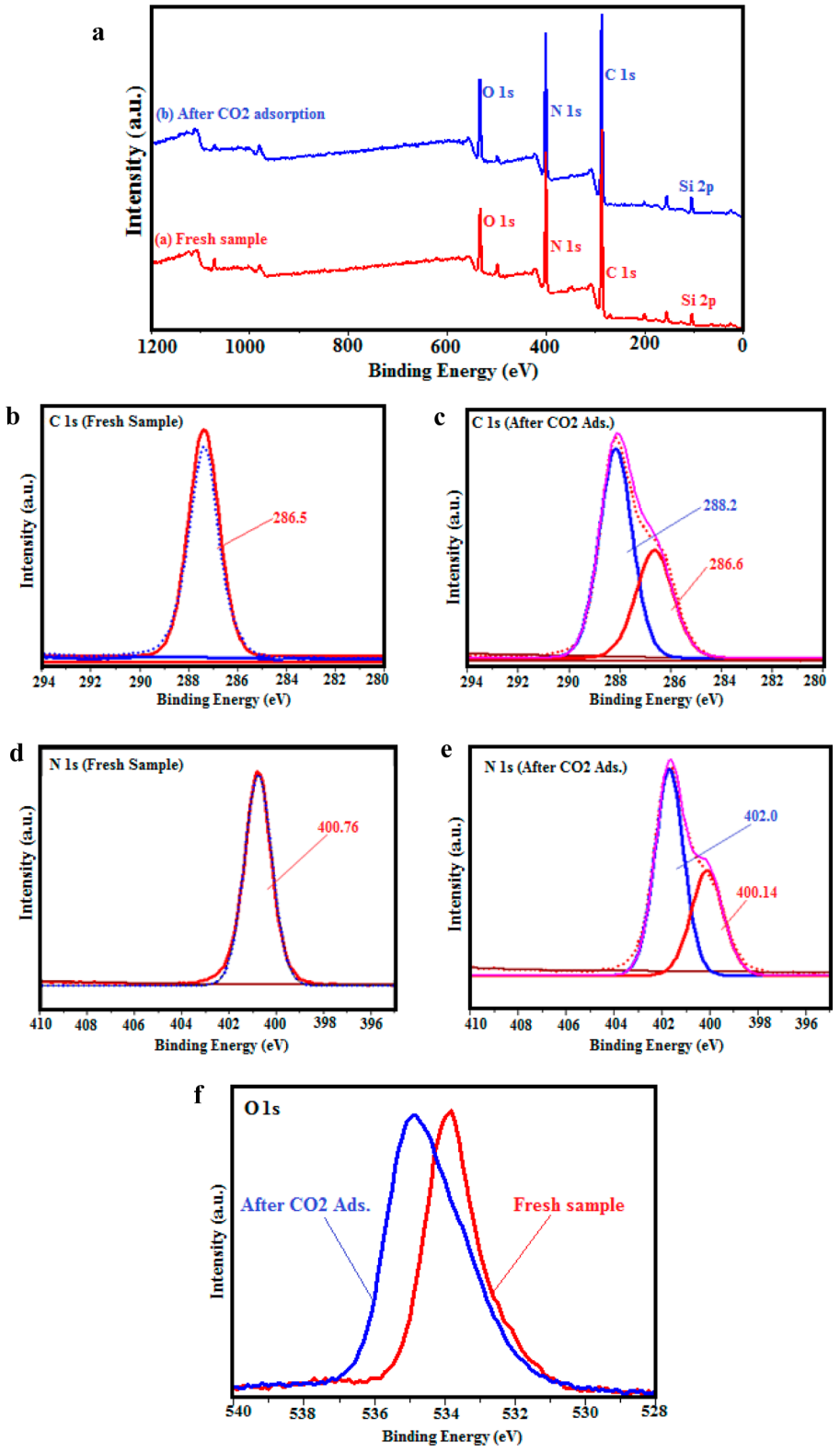

Figure 3. X-ray photoelectron spectra of PEI-10k/MPS before CO_2 and after CO_2 adsorption.

Representative SEM images are shown in Figure 1. The average pore size of the MPS is about 56 nm. The images in Figure 1b,c show that PEI molecules are immobilized inside the mesoporous foam cells with some on the external surfaces. Nonetheless, the hierarchical porous structure within and between the sorbent particles is retained facilitating diffusion of CO_2 gas in the sorbent. Considering that the silica foam particles are microns in size with inter- and intraparticle voids in tens to hundreds of microns, the loosely packed sorbent powders can be used in a fixed bed or a fluidized bed reactor with relatively low flow rates to minimize potential pressure drop during the operation.

Figure 2 shows the FTIR spectra for the sample before and after CO_2 adsorption. A strong, broad peak near 3350 cm^{-1} is

DOI: 10.1021/acs.langmuir.5b00189
Langmuir 2015, 31, 3569−3576

visible in both cases most likely due to stretching of the amine groups of the immobilized PEI.[34] Two weak peaks for C−H stretching of methylene fragments of PEI appear at 2935 and 2835 cm^{-1}, respectively. The peaks at 1575 and 1485 cm^{-1} are likely due to the bending deformation of the NH_3^+ group.[34] All the samples show a strong absorption band around 1110 cm^{-1} from the Si−O−Si asymmetric stretching vibrations. After CO_2 adsorption, the sorbent shows two new absorption band at 1650 and 1414 cm^{-1}, which can be assigned to N−H deformation in RNH_3^+ and NCOO skeletal vibration, respectively, indicative of the formation of carbamates during CO_2 adsorption.[34,35] The weak, broad IR peak at 1325 cm^{-1} (Figure 2b) could be due to NCOO skeletal vibration.[34,35] These results indicate that CO_2 adsorbs on the PEI-MPS through the formation of alkalammonium carbamate, as suggested previously for primary and secondary amine groups:[37−39]

$$CO_2 + 2RNH_2 \rightarrow RNHCO_2^- + RNH_3^+ \quad (1)$$

$$CO_2 + 2R_1R_2NH \rightarrow R_1R_2NCO_2^- + R_1R_2NH_2^+ \quad (2)$$

It is worth mentioning that all the work reported in this paper was carried out under dry CO_2 conditions, which does not favor the formation of bicarbonate. The weak, broad IR peak at 1325 cm^{-1} (Figure 2b) could be due to NCOO skeletal vibration,[34,35] although we cannot exclude the formation of bicarbonate, which is favored in the presence of moisture as shown in the equation

$$CO_2 + 2R{-}NH_2 + H_2O \rightarrow R{-}NH_3^+HCO_3^- \quad (3)$$

XPS was used to investigate surface composition before and after exposure to CO_2. As expected, XPS of the PEI/MPS revealed the presence of N, C, O, and Si. The reaction between primary and secondary amines with CO_2 leads to the formation of carbamate as presented in eqs 1 and 2, respectively. The chemical reaction mechanism between primary or secondary amino groups with CO_2 proceeds via a zwitterion intermediate.[38−41] The reaction pathway consists of two steps. First, a zwitterion is formed between the amino group and the carbon dioxide molecule. Then, a base is necessary to stabilize the zwitterion and to obtain a carbamate as a final product. If water is present in the media, it can act as a base, receiving the proton transferred by the zwitterion (eq 3). But in this case, as no other base is present, another amino group acquires a positive charge forming the carbamate according to reactions 1 and 2 for primary and secondary amines, respectively.

For carbamate the end group contains C and N as well as O atomic species, and hence single peak features at 286, 400, and 534 eV were measured and analyzed in the respective 1s spectra. Figure 3a shows the XPS spectra of PEI-10K/MS before and after CO_2 treatment. The detailed C 1s, O 1s, and N 1s core-level spectra corresponding to PEI-10K/MPS/CO_2 are also shown in Figure 3b−f. The C 1s spectra of the PEI-10K/MPS occurs at 286 eV, which is a typical combination of C−C and C−H boding. When covered with CO_2, a new peak appeared at 288 eV (Figure 3c), possibly due to the N−CO_2 surface carbonyl chemical bonds.[42,43] The nitrogen 1s appears at a binding energy consistent with a typical amine functional group (400 eV). After CO_2 adsorption, a new peak appears at 402 eV (Figure 3e) that could be due to the protonated nitrogen associated with the formation of the carbamate ion.[41,44] Figure 3f shows that the XPS oxygen peak is shifted from 334 to 335 eV due to CO_2 adsorption. The 334 eV peak is due to O 1s bonded to Si; on the other hand, the 335 eV peak is assigned to O 1s of chemisorbed CO_2. The shift to relatively high binding energy of the O 1s is attributed due to double-bond character of the chemisorbed CO_2.

The thermal properties of the sorbents were investigated by TGA and DSC. The differential TGA profiles are shown in Figure 4. The minor mass loss below 101 °C could be due to

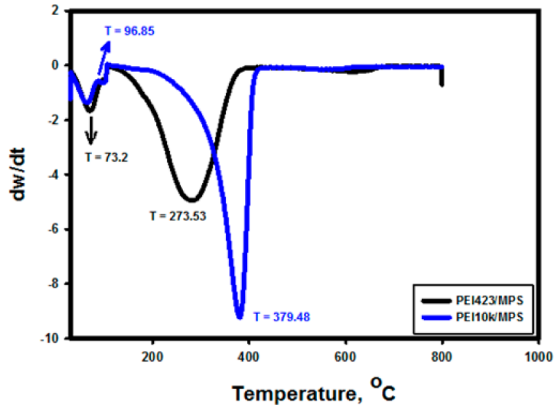

Figure 4. Thermogravimetric (TGA) graphs of PEI432/MPS and PEI10k/MPS.

the desorption of H_2O and CO_2, which are expected to be present on the sorbent due to exposure to air. Thus, to desorb any preadsorbant, the samples were heated to 110 °C in N_2 for ~30 min before CO_2 adsorption measurements. The differential TGA peaks in Figure 4 were broad and centered at 273 and 379 °C for PEI-423/MPS and PEI-10K/MPS, respectively. These peaks were due to the vaporization of shorter chain polyamine molecules and/or the decomposition of the longer PEI molecules at elevated temperatures.[18]

The differential scanning calorimetry (DSC) thermogram of amine/MPS is consistent with the TGA analysis (Figure 5).

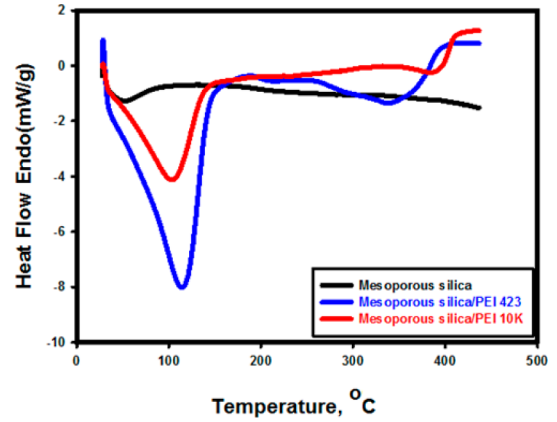

Figure 5. Differential scanning calorimetry (DSC) thermogram of PEI/MPS.

The peak above 100 °C is due to desorption of H_2O and CO_2. The peaks at 350 and 400 °C for PEI-423/MPS and PEI-10K/MPS, respectively, indicate the start of evaporation and/or decomposition of the adsorbed amines, which were observed as weight loss at high temperatures in Figure 4.

Despite the similar nitrogen content, PEI-10K/MPS showed lower CO_2 capacity than PEI-423/MPS, as shown in Figure 6. This difference in sorbent capacity may be related to the

DOI: 10.1021/acs.langmuir.5b00189
Langmuir 2015, 31, 3569−3576

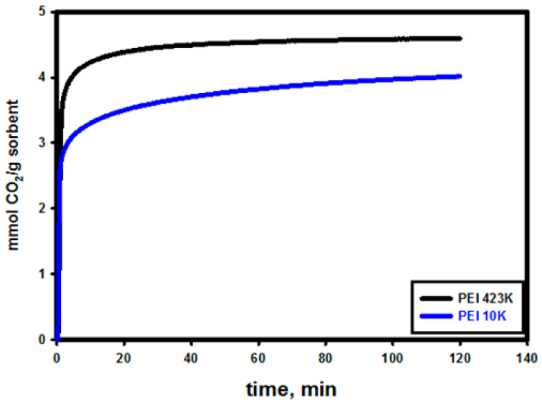

Figure 6. Comparison between the adsorption of CO_2 on PEI-432/MPS and PEI-10K/MPS at 75 °C.

molecular structure of PEI-423 and PEI-10K. PEI-423 is a linear polyethylenimine while PEI-10K is a hyperbranched polymer with a ratio of primary, secondary, and tertiary amine about 1:2:1 (as described by the chemical vendor). In dry CO_2, only primary and secondary amines react with CO_2.[45] Moreover, the larger molecular weight of PEI-10K results in higher polymer chain rigidity and thus higher CO_2 diffusion resistance, leading to lower CO_2 capacity. It is interesting to notice that the adsorbed CO_2 can be kept by the sorbent for several days at room temperature. Indeed, the TGA results showed that certain amount of CO_2 could still be stored in the sorbent over 24 h at 35 °C under flowing nitrogen, suggesting the sorbents can be potentially used for CO_2 storage at relatively low temperatures.

3.2. CO_2 Adsorption–Desorption Profiles. The CO_2 adsorption–desorption performance was measured after sorbent activation in nitrogen at 110 °C for about 30 min. Figures 7a and 7b respectively show the adsorption–desorption profiles of PEI-423/MPS and PEI-10K/MPS at different temperatures for five consecutive cycles. Once the sorbent is exposed to CO_2 an instantaneous mass gain was seen by the samples due to CO_2 adsorption. It is clear that adsorption on both sorbents is a two-stage process: the first step exhibited an exponential weight gain that took about 5–10 min followed by a second, much slower process that leveled off at maximum values depending on temperature. The optimal adsorption temperature for PEI-423/MPS and PEI-10K/MPS was 75 and 85 °C, respectively, under the test conditions. The relatively higher temperature of maximum adsorption for PEI-10/MPS could be attributed to lower flexibility of the polyamine chains of PEI-10K and higher steric effect exhibited by such branched molecules leading to a higher activation temperature. Figure 8

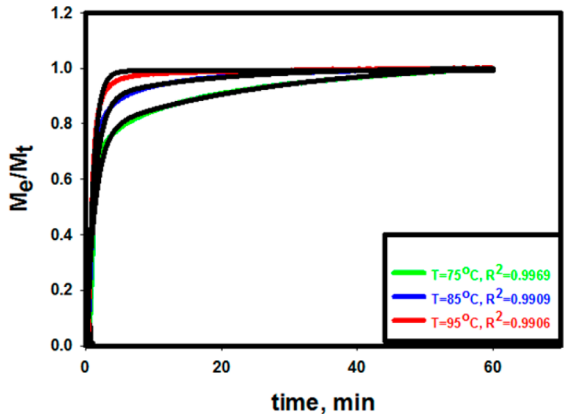

Figure 8. Fitting results of CO_2 adsorption on PEI-423/MPS at various temperatures (color and black curves correspond to experimental and theoretical, respectively).

also shows that after reaching an optimal adsorption temperature, the sorbent capacity declined with further increase in temperature. This decline indicates that the adsorption–desorption of CO_2 is a reversible process, where increasing the temperature decreases the net amount of CO_2 adsorbed due to simultaneous desorption. When the gas flow was switched from CO_2 to N_2, there was a noticeable mass loss due to CO_2 desorption. The process of desorption is also a two-stage process; the first was a very fast exponential decay while the second was slower and extended to as long as more than 24 h at a lower temperature. During the five adsorption–desorption consecutive cycles there was no sign of deteriorating the sorbent activity for CO_2 capture. Indeed, the stability of other PEI-functionalized solid sorbents has been reported for up to 100 adsorption–desorption cycles.[17,18] The initial fast

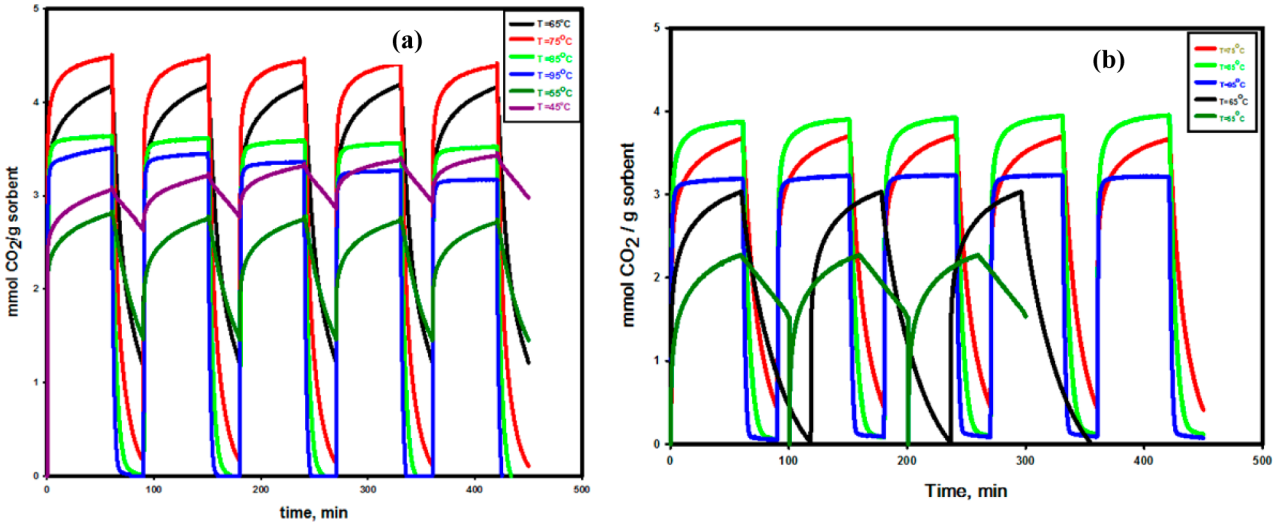

Figure 7. CO_2 adsorption–desorption cycles at various temperatures for (a) PEI-423/MPS and (b) PEI-10K/MPS.

DOI: 10.1021/acs.langmuir.5b00189
Langmuir 2015, 31, 3569–3576

step in the profiles of Figure 7 could be assigned to surface adsorption, followed by a slower process, which could be attributed to CO_2 diffusion into the MPS particles and amine layers with increasing diffusion resistance after reacting with CO_2.

To get a deeper insight into the sorption process of the sorbents, the following double-exponential model was adopted to describe the kinetics of CO_2 adsorption on PEI/MPS sorbents:

$$\frac{M_t}{M_e} = A_S(1 - \exp(-k_S t)) + A_D(1 - \exp(-k_D t)) \quad (4)$$

This mathematical model has been described and utilized earlier by Kondo et al.[46] and Fletcher et al.[47] in studying other adsorption processes. In eq 4, M_t and M_e represent the experimental mass gain due to CO_2 sorption at time t and after reaching equilibrium, respectively. The experimental M_e, M_t, and the time of adsorption, t, have been fitted with eq 4 using the Sigma Plot 2012 software with a tolerance value set at 1×10^{-10}. As shown in eq 4, there are four fitting parameters, namely, A_S, A_D, k_S, and k_D. A_S and A_D are defined as the relative contributions of surface and diffusion barriers, respectively, controlling the overall adsorption process, where the sum of A_S and A_D equals to 1, and k_S and k_D are defined as the corresponding surface and diffusion rate constants, respectively. The fitting results of the double-exponential model along with the corresponding experimental results are summarized in Figure 8. The fitting results show a good fit of the double-exponential model on the experimental results (R^2 values >0.99 as shown in the graph). In a sharp contrast, when the data were fit to an Arrhenius equation for determining the adsorption activation energies, no good fits were obtained. The nonlinearity of the Arrhenius plot could be attributed to the reversibility of the adsorption−desorption CO_2.[45,46] Expectedly, as shown in Table 1, the first rate constant, k_S, due to surface adsorption at all temperatures was always higher than the diffusion rate constant, k_D. Table 1 also shows that k_S and k_D for PEI-423/MPS were always higher than the corresponding values of PEI-10K/MPS revealing faster CO_2 adsorption on PEI-423/MPS than PEI-10K/MPS.

Table 1. Rate Constants for CO_2 Adsorption on PEI/MPS[a]

	surface rate constants (min^{-1})		diffusion rate constants (min^{-1})	
temp (K)	k_S(PEI-423/MPS)	k_S(PEI-10K/MPS)	k_D(PEI-423/MPS)	k_D(PEI-10K/MPS)
318	1.5970		0.0367	
328	1.5071	0.1361	0.0372	0.0278
338	1.6753	0.1513	0.0373	0.0318
348	1.7286	0.7266	0.0599	0.0372
358	4.3646	0.7853	1.5969	0.0583
368	8.3132	5.4170	2.0806	1.1984

[a]Rate constants k_S and k_D were calculated by fitting eq 2 to the CO_2 adsorption profiles of Figure 7a,b.

In contrast, the desorption profiles were fitted using the simple first-order kinetic equation

$$M_{des} = M_0 e^{-k_{des} t} \quad (5)$$

where M_{des} is the mass of CO_2 desorbed at time t and M_0 the initial mass of adsorbed CO_2, i.e., the mass at maximum adsorption, and k_{des} is the desorption rate constant. The desorption processes obeyed the Arrhenius relation as shown in Figure 9. From the slope of Figure 9, the activation energy for

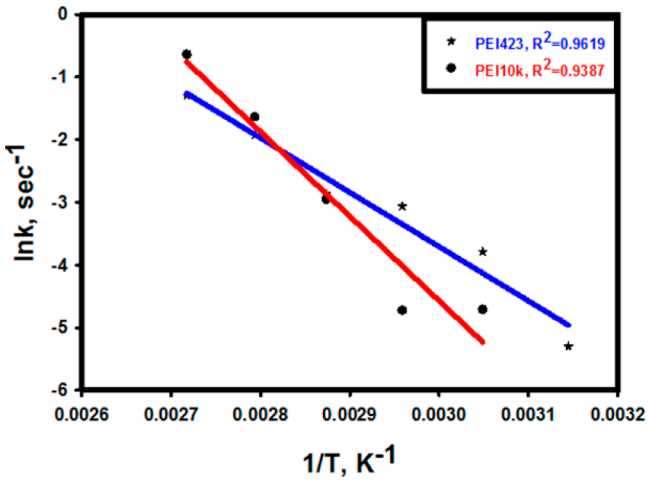

Figure 9. Arrhenius relationships for CO_2 desorption off PEI-423/MPS and PEI-10K/MPS.

CO_2 desorption from PEI-423/MPS was 64.3 kJ mol^{-1}, consistent with the results of other supported amine sorbent using mesoporous foam as the support.[18] Note that the calculated energy required for desorption of PEI-10K/MPS is 140.7 kJ mol^{-1}, much higher than that of PEI-423/MPS. One potential explanation is the presence of large amounts of tertiary amine groups in PEI-10K (about one-fourth according to the specification of the manufacturer), which is inactive toward dry CO_2.[45] In addition, the steric effect exerted by the branched PEI-10K may also attribute to the higher activation energy of CO_2 desorption from PEI-10K/MPS.

4. CONCLUSIONS

We have evaluated the performance of amine functionalized sorbents prepared using a pilot-scale mesoporous silica foam as sorbent support. The sorbents exhibited high CO_2 sorption capacity and fast adsorption rate. The sorption kinetics was fitted with a double-exponential model from which the rate constants for the surface and diffusion interaction of the CO_2/PEI-MPS were evaluated. Desorption of CO_2 followed first-order kinetics with activation energies of 64.3 and 140.7 kJ mol^{-1} for CO_2 desorption from PEI-423/MPS and PEI-10K/MPS, respectively. The sorption rate and activation energy results suggest the sorbent performance is strongly related to the structure of the immobilized amine.

AUTHOR INFORMATION

Corresponding Author

*E-mail mmkhader@qu.edu.qa; Ph (+974) 55825744 (M.M.K.).

Notes

The authors declare no competing financial interest.

ACKNOWLEDGMENTS

This paper was made possible by an NPRP Grant #5-1437-1-243 from the Qatar National Research Fund (a member of Qatar Foundation) and generous research computing support from Cornell University. The statements made herein are solely the responsibility of the authors.

DOI: 10.1021/acs.langmuir.5b00189
Langmuir 2015, 31, 3569−3576

REFERENCES

(1) Rao, A. B.; Rubin, E. S. A technical, economic, and environmental assessment of amine-based CO_2 capture technology for power plant greenhouse gas control. *Environ. Sci. Technol.* **2002**, *36*, 4467−4475.

(2) Wolsky, A. M.; Daniels, E. J.; Jody, B. CO_2 capture from the flue gas of conventional fossil-fuel-fired power plants. *J. Environ. Prog.* **1994**, *13*, 214−219.

(3) Mandal, B. P.; Biswas, A. K.; Bandyopadhyay, S. S. Absorption of carbon dioxide into aqueous blends of 2-amino-2-methyl-1-propanol and diethanolamine. *Chem. Eng. Sci.* **2003**, *58*, 4137−4144.

(4) Mandal, B. P.; Bandyopadhyay, S. S. Absorption of carbon dioxide into aqueous blends of 2-amino-2-methyl-1-propanol and monoethanolamine. *Chem. Eng. Sci.* **2006**, *61*, 5440−5447.

(5) Maurin, G.; Lewellyn, P. L.; Bell, R. G. Adsorption mechanism of carbon dioxide in faujasites: grand canonical Monte Carlo simulations and microcalorimetry measurements. *J. Phys. Chem. B* **2005**, *109*, 16084−16091.

(6) Guerrero, R. S.; Belmabkhout, Y.; Sayari, A. Modeling CO_2 adsorption on amine-functionalized mesoporous silica: 1. A semi-empirical equilibrium model. *Chem. Eng. J.* **2010**, *161*, 173−181.

(7) Zhilin, L.; Yang, T.; Kai, Z.; Yan, C.; Wei-ping, P. CO_2 adsorption properties and thermal stability of different amine-impregnated MCM-41 materials. *J. Fuel Chem. Technol.* **2013**, *41*, 469−476.

(8) Yang, S. T.; Kim, J. Y.; Kim, J.; Ahn, W. S. CO_2 capture over amine-functionalized MCM-22, MCM-36 and ITQ-2. *Fuel* **2012**, *97*, 435−442.

(9) Bhagiyalakshmi, M.; Yun, L. J.; Anuradha, R.; Jang, H. T. Synthesis of chloropropylamine grafted mesoporous MCM-41, MCM-48 and SBA-15 from rice husk ash: Their application to CO_2 chemisorption. *J. Porous Mater.* **2010**, *17*, 475−484.

(10) Yanfang, F.; Ryan, P. L.; Ying, L.; Fateme, R.; William, J. K.; Christopher, W. J. Evaluation of CO_2 adsorption dynamics of polymer/silica supported poly(ethylenimine) hollow fiber sorbents in rapid temperature swing adsorption. *Int. J. Greenhouse Gas Control* **2014**, *21*, 61−71.

(11) Mustafa, A. A.; Ratayakorn, K.; Christopher, W. J. Guanidinylated poly(allylamine) supported on mesoporous silica for CO_2 capture from flue gas. *Fuel* **2014**, *121*, 79−85.

(12) Dong, H. J.; Hyunchul, J.; Dong, K. S.; Chang, H. L.; Sung, H. K. Effect of amine structure on CO_2 adsorption over tetraethylene-pentamine impregnated poly methyl methacrylate supports. *Sep. Purif. Technol.* **2014**, *125*, 187−193.

(13) Young, G. K.; Hyun, J. L.; Hyun, C. O.; Ung, S. C. Amines immobilized double-walled silica nanotubes for CO_2 capture. *J. Hazard. Mater.* **2013**, *250*, 53−60.

(14) Ku, Y. G.; Lee, H. J.; Kim, J. Y.; Choi, U. S. Hierarchically porous aminosilica monolith as a CO_2 adsorbent. *ACS Appl. Mater. Interfaces* **2014**, *6*, 12988−12996.

(15) Wang, K.; Shang, H.; Yan, L. L. X.; Yan, Z.; Liu, C.; Zha, Q. Efficient CO_2 capture on low-cost silica gel modified by polyethyleneimine. *J. Nat. Gas Chem.* **2012**, *21*, 319−323.

(16) Brilman, D. M. F.; Veneman, R. Capturing atmospheric CO_2 using supported amine sorbents. *Energy Procedia* **2013**, *37*, 6070−6078.

(17) Qi, G.; Wang, Y.; Estevez, L.; Duan, X.; Anako, N.; Park, A. A.; Li, W.; Jones, C. W.; Giannelis, E. P. High efficiency nanocomposite sorbents for CO_2 capture based on amine-functionalized mesoporous capsules. *Energy Environ. Sci.* **2011**, *4*, 444−452.

(18) Qi, G.; Fu, L.; Choi, B. H.; Giannelis, E. P. Efficient CO_2 sorbents based on silica foam with ultra-large mesopores. *Energy Environ. Sci.* **2012**, *5*, 7368−7375.

(19) Chen, C.; Son, W.-J.; Youb, K.-S.; Ahn, J.-W.; Ahn, W.-S. Carbon dioxide capture using amine-impregnated HMS having textural mesoporosity. *Chem. Eng. J.* **2010**, *161*, 46−52.

(20) Labreche, Y.; Lively, R. P.; Rezaei, F.; Chen, G.; Jones, C. W.; Koros, W. J. Post-spinning infusion of poly(ethyleneimine) into polymer/silica hollow fibre sorbents for carbon dioxide capture. *Chem. Eng. J.* **2013**, *221*, 166−175.

(21) Kim, J.-Y.; Kim, J.; Yang, S.-T.; Ahn, W.-S. Mesoporous SAPO-34 with amine-grafting for CO_2 capture. *Fuel* **2013**, *108*, 515−520.

(22) Dutcher, B.; Fan, M.; Cui, S.; Shen, X−D.; Kong, Y.; Russell, A. G.; McCurdy, P.; Giotto, M. Characterization and stability of a new, high-capacity amine-functionalized CO_2 sorbent. *Int. J. Greenhouse Gas Control* **2013**, *18*, 51−56.

(23) Cheung, O.; Bacsik, Z.; Liu, Q.; Mace, A.; Hedin, N. Adsorption kinetics for CO_2 on highly selective zeolites NaKA and nano-NaKA. *Appl. Energy* **2013**, *112*, 1326−1336.

(24) Xu, X.; Zhao, X.; Sun, L.; Liu, X. Adsorption separation of carbon dioxide, methane and nitrogen on monoethanol amine modified b-zeolite. *J. Nat. Gas Chem.* **2009**, *18*, 167−172.

(25) Rashidi, N. A.; Yusup, S.; Loong, L. H. Kinetic studies on carbon dioxide capture using activated carbon. *Chem. Eng. Trans.* **2013**, *35*, 361−366.

(26) Guo, B.; Chang, L.; Xie, K. Adsorption of carbon dioxide on activated carbon. *J. Nat. Gas Chem.* **2006**, *15*, 223−229.

(27) Dantas, T. L. P.; Luna, F. M. T.; Silva, I. J., Jr.; de Azevedo, D. C. S.; Grande, C. A.; Rodrigues, A. E.; Moreira, R. M. Carbon dioxide−nitrogen separation through adsorption on activated carbon in a fixed bed. *Chem. Eng. J.* **2011**, *169*, 11−19.

(28) Shafeeyan, M. S.; Daud, W.; Houshmand, A.; Shamiri, A. A review on surface modification of activated carbon for carbon dioxide adsorption. *J. Anal. Appl. Pyrolysis* **2010**, *89*, 143−151.

(29) Auta, M.; Amat, N. D.; Mohd Din, A. T.; Hameed, B. H. Fixed-bed column adsorption of carbon dioxide by sodium hydroxide modified activated alumina. *Chem. Eng. J.* **2013**, *233*, 80−87.

(30) Chen, C.; Ahn, W. S. CO_2 capture using mesoporous alumina prepared by a sol−gel process. *Chem. Eng. J.* **2011**, *166*, 646−651.

(31) Thote, J. A.; Chatti, R. V.; Iyer, K. S.; Kumar, V.; Valechha, A. N.; Labhsetwar, N. K.; Biniwale, R. B.; Yenkie, M. K. N.; Rayalu, S. S. N-doped mesoporous alumina for adsorption of carbon dioxide. *J. Environ. Sci.* **2012**, *24*, 1979−1984.

(32) Vajiheh, N.; May, B. H. Development of dual layer of ZIF-8/PEBAX-2533 mixed matrix membrane for CO_2 capture. *J. Membr. Sci.* **2014**, *459*, 244−455.

(33) Giannelis, E. P.; Fu, L.; Qi, G. Metal oxide foam, amine functional solid sorbent, methods and applications. Patent Application US 20130338001 A1, Dec 19, 2013.

(34) Bacsik, Z.; Ahlsten, N.; Ziadi, A.; Zhao, G.; Garcia-Bennett, A. E.; Martín-Matute, B.; Hedin, N. Mechanisms and kinetics for sorption of CO_2 on bicontinuous mesoporous silica modified with n-propylamine. *Langmuir* **2011**, *27*, 11118−11128.

(35) Wang, X. X.; Schwartz, V.; Clark, J. C.; Ma, M. L.; Overbury, S. H.; Xu, X. C.; Song, C. S. Infrared study of CO_2 sorption over "molecular basket" sorbent consisting of polyethylenimine-modified mesoporous molecular sieve. *J. Phys. Chem. C* **2009**, *113*, 7260−7268.

(36) Hicks, J. C.; Drese, J. H.; Fauth, D. J.; Gray, M. L.; Qi, G.; Jones, C. W. Particle-scale CO_2 adsorption kinetics modeling considering three reaction mechanisms. *J. Am. Chem. Soc.* **2008**, *130*, 2902−2903.

(37) Schladt, M.; Fiburn, T. P.; Helble, J. J. Supported amine sorbents under temperature swing absorption for CO_2 and moisture capture. *Ind. Eng. Chem. Res.* **2007**, *46*, 1590−1597.

(38) McCann, N.; Phan, D.; Fernandes, D.; Maeder, M. A Systematic Investigation of Carbamate Stability Constants y 1H NMR. *Int. J. Greenhouse Gas Control* **2011**, *5*, 396−400.

(39) Sanz, R.; Calleja, G.; Arencibia, A.; Sanz-Pèrez, E. S. CO_2 adsorption on branched polyethyleneimine-impregnated mesoporous silica SBA-15. *Appl. Surf. Sci.* **2010**, *256*, 5323−5328.

(40) Hiyoshi, N.; Yogo, K.; Yashima, T. Adsorption characteristics of carbon dioxide on organically functionalized SBA-15. *Microporous Mesoporous Mater.* **2005**, *84*, 357−365.

(41) Aresta, M.; Quaranta, E. Role of the macrocyclic polyether in the synthesis of N-alkylcarbamate esters from primary amines, CO_2 and alkyl halides in the presence of crown-ethers. *Tetrahedron* **1992**, *48*, 1515−1530.

(42) Ameen, A. P.; Ward, R. J.; Short, R. D.; Beamson, G.; Briggs, D. A high-resolution X-ray photoelectron spectroscopy study of trifluoro-

DOI: 10.1021/acs.langmuir.5b00189
Langmuir 2015, 31, 3569−3576

acetic anhydride labelling of hydroxyl groups: demonstration of the β shift due to -OC(O)CF_3. *Polymer* **1993**, *34*, 1795−1799.
(43) Briggs, D.; Beamson, G. Primary and secondary oxygen-induced C1 s binding energy shifts in X-ray photoelectron spectroscopy of polymers. *Anal. Chem.* **1992**, *64*, 1729−1736.
(44) El Nahhal, I. M.; Chehimi, M. M.; Cordier, C.; Dodin, G. XPS, NMR and FTIR structural characterization of polysiloxane-immobilized amine ligand systems. *J. Non-Cryst. Solids* **2000**, *275*, 142−146.
(45) Al-Marri, M. J.; Khader, M. M.; Giannelis, E. P.; Shibl, M. F. Optimization of selection of chain amine scrubbers for CO_2 capture. *J. Mol. Model.* **2014**, *20*, 2518−2528.
(46) A; Kojima, N.; Kajiro, H.; Noguchi, H.; Hattori, Y.; Okino, F.; Maeda, K.; Ohba, T.; Kaneko, K.; Kanoh, H. Gas adsorption mechanism and kinetics of an elastic layer-structured metal-organic framework. *J. Phys. Chem. C* **2012**, *116*, 4157−4162.
(47) Fletcher, A. J.; Cussen, E. J.; Bradshaw, D.; Rosseinsky, M. J.; Thomas, K. M. Adsorption of gases and vapors on Nanoporous Ni^{+2}(4,4′-bipyridine)$_3$(NO_3)$_4$ metal-organic framework materials templated with methanol and ethanol: Structural effects in adsorption kinetics. *J. Am. Chem. Soc.* **2004**, *126*, 9750−9759.

DOI: 10.1021/acs.langmuir.5b00189
Langmuir 2015, 31, 3569−3576